

MONASH UNIVERSITY

HONOURS THESIS

# Thin oxides in graphene devices



IMAGE  
PLACEHOLDER

---

Supervisors:

Michael Fuhrer  
Semonti Bhattacharyya

---

Physics Honours, Monash University  
Student ID: 24121843



# Abstract

I present a review of the use of graphene in electronic devices, both in its shortfalls and exciting properties. The electronic structure is detailed, along with various scattering sources that affect electron transport and ultimately the goal of room temperature, electronic devices. Considering heterostructures and the use of other materials to enhance graphene, I discuss the potential use of hafnium dioxide, and other oxides, as an excellent gate dielectric material for potential use in graphene field-effect devices.

# Contents

<b>Abstract</b>	<b>1</b>
<b>Foreword</b>	<b>4</b>
<b>1 Introduction</b>	<b>5</b>
1.1 Preface . . . . .	5
1.2 Transistors - the field effect . . . . .	5
1.2.1 Conductivity in FETs . . . . .	5
1.2.2 Mobility in FETs . . . . .	5
1.3 Graphene . . . . .	5
1.3.1 Electronic properties . . . . .	5
1.3.1.1 Hybridisation . . . . .	6
1.3.1.2 Electronic dispersion . . . . .	6
1.3.1.3 Charged puddling . . . . .	6
1.4 Transport and scattering in graphene . . . . .	6
1.4.1 Charged impurities . . . . .	6
1.4.2 Phonon scattering . . . . .	6
1.4.3 Dielectric screening . . . . .	6
1.4.3.1 Charge screening . . . . .	6
1.4.3.2 Fine structure constant . . . . .	6
1.4.3.3 Tuning the fine structure constant . . . . .	6
1.4.3.4 High $\kappa$ materials . . . . .	6
1.4.4 Remote phonon scattering . . . . .	6
1.5 . . . . .	6
<b>2 Experimental techniques</b>	<b>7</b>
2.1 Fabrication . . . . .	7
2.1.1 Graphene . . . . .	8
2.1.2 Chemical vapour deposition graphene . . . . .	8
2.1.3 Exfoliation of graphene . . . . .	9
2.1.4 Lithography . . . . .	9
2.1.4.1 Spin coating photoresists . . . . .	10
2.1.4.2 Exposure . . . . .	11
2.1.4.3 Developers . . . . .	12
2.1.4.4 Contact pad dimensions . . . . .	12
2.1.5 UV Ozone surface preparation . . . . .	13
2.1.6 Deposition . . . . .	13
2.1.6.1 Oxide Protection . . . . .	14
2.1.7 Lift-off . . . . .	14
2.1.7.1 Ultrasonication . . . . .	14
2.1.8 Argon/Hydrogen Annealing . . . . .	15
2.1.9 PCB board mounting . . . . .	15

2.1.10 Oxide stamping . . . . .	16
2.2 Measurement techniques . . . . .	16
2.2.1 4 probe measurements . . . . .	16
2.2.1.1 Sourcemeters . . . . .	17
2.2.1.2 Lock-in amplifiers . . . . .	18
2.2.2 Probe station . . . . .	19
2.2.2.1 Vacuum . . . . .	19
2.2.2.2 Temperature control . . . . .	19
2.2.2.3 Static Discharge . . . . .	20
2.2.2.4 Probes . . . . .	20
<b>3 Characterisation of graphene</b>	<b>21</b>
3.1 Raman spectroscopy . . . . .	21
3.1.1 Raman in graphite . . . . .	21
3.1.2 Raman in graphene . . . . .	21
3.2 Optical microscopy . . . . .	23
3.2.1 Contrast imaging . . . . .	24
<b>4 Electrical measurements of pristine graphene</b>	<b>26</b>
4.1 CVD . . . . .	26
4.2 Exfoliated . . . . .	26
4.2.1 hBN transfer . . . . .	26
<b>5 Thin oxides</b>	<b>27</b>
5.1 Printing . . . . .	27
5.1.1 Al <sub>2</sub> O <sub>3</sub> . . . . .	27
5.1.2 SnO . . . . .	27
5.1.3 Bi <sub>2</sub> O <sub>3</sub> . . . . .	27
5.2 Smearing . . . . .	27
5.2.1 Ga <sub>2</sub> O <sub>3</sub> . . . . .	27
<b>6 Conclusion</b>	<b>28</b>
6.1 Future direction . . . . .	28
6.2 Concluding remarks . . . . .	28
<b>List of Figures</b>	<b>29</b>
<b>List of Tables</b>	<b>30</b>
<b>7 References</b>	<b>31</b>
<b>Appendices</b>	<b>34</b>
<b>A Raman spectroscopy samples</b>	<b>35</b>
<b>B Labview programs</b>	<b>36</b>

# Foreword

This thesis serves the purpose presenting the conclusions of my research into thin oxides on graphene. I will be arguing , and how that fits into a bigger picture of materials science and particular applications.

In chapter 1, I will outline what I hope to achieve in this project. I begin by discussing the theoretical properties of graphene and why it has attracted so much interest as an electronic material. I will also describe some challenges facing new computing technologies, including the use of dielectrics, and how my work contributes to realising solutions to new generations of this technology. I will outline a theoretical and experimental summary of the results to date seen in introducing dielectrics to graphene.

In chapter 2, I describe the various ways of producing and identifying graphene in lab use, and the characterisations I have conducted. This will include our use of atomic force microscopy (AFM), optical microscopy and Raman spectroscopy.

I will then describe the devices and measurements I have made in chapter 3. This will regard connections to devices, which allow the measurements I have perform, and the processes used to fabricate our devices. I have made graphene devices using lithography and evaporation methods, to create electrical contacts. I will also describe the oxides I have investigated in this chapter, and the methods I have used to transfer them.

In chapter 4 I will present the data and results from my measurements of the respective devices which will be placed on  $\text{SiO}_2$ . The results to here will be compared alongside data after stamping the same devices with thin oxides in chapter 5.

# **Chapter 1**

## **Introduction**

### **1.1 Preface**

The mechanical exfoliation of atomically thin materials in 2004 sparked a flurry of research into many materials with unique properties. Graphene, the first of these, rose to prominence in research and has begun finding applications in industrial contexts.

Materials that are two dimensional restrict the movement of electrons to a plane. Because of this, these materials exhibit unique electronic properties. A clear example of this is a hexagonal lattice of carbon atoms, or graphene, which gives rise to a 'dirac' point in the band structure (see section 1.3.1.2).

### **1.2 Transistors - the field effect**

#### **1.2.1 Conductivity in FETs**

#### **1.2.2 Mobility in FETs**

### **1.3 Graphene**

#### **1.3.1 Electronic properties**

Why is it a good conductor?

1.3.1.1 Hybridisation

1.3.1.2 Electronic dispersion

1.3.1.3 Charged puddling

## 1.4 Transport and scattering in graphene

1.4.1 Charged impurities

1.4.2 Phonon scattering

1.4.3 Dielectric screening

1.4.3.1 Charge screening

1.4.3.2 Fine structure constant

1.4.3.3 Tuning the fine structure constant

1.4.3.4 High  $\kappa$  materials

1.4.4 Remote phonon scattering

## 1.5

# Chapter 2

## Experimental techniques

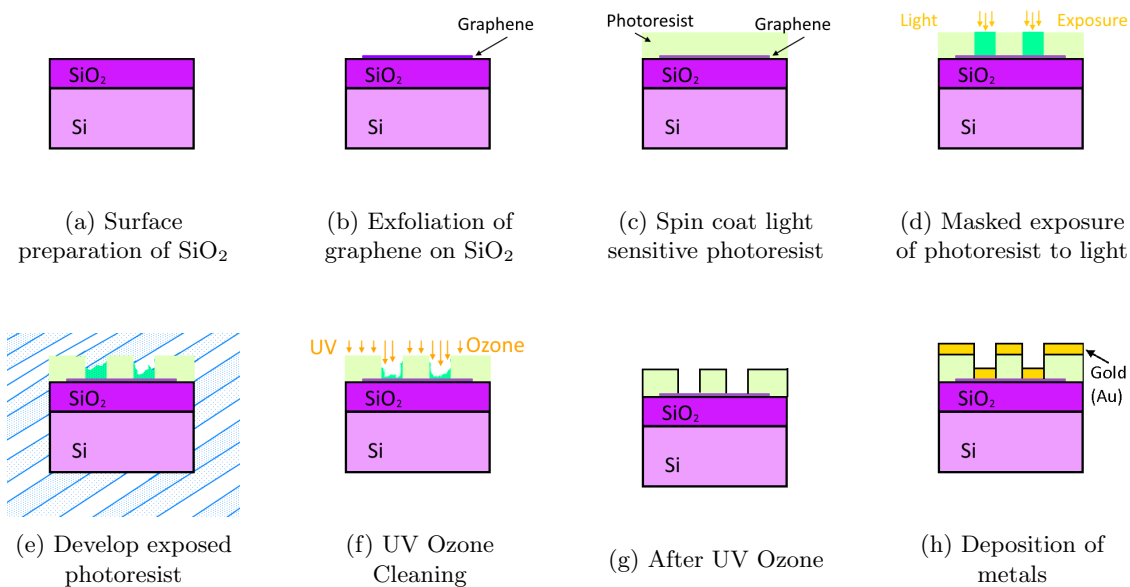
Two aspects are involved in performing electronic measurements of materials, namely fabrication and measurement techniques.

Physical devices containing graphene need to be fabricated allow measurements to take place. This primarily deals with the production of materials (graphene, oxides) and the processes to develop connectable devices. Some of the tools and techniques used include lithography, electron beam evaporation, and etching. The processes used in this project are detailed in section 2.1.

To measure the properties of graphene, particular experimental methods and procedures are required to control the environment and obtain useful data. Section 2.2 primarily deals with the operation of the experimental apparatus used to measure the electronic properties of graphene.

### 2.1 Fabrication

To create graphene devices where we can measure the electronic properties referenced in sections 1.2 and 1.3.1, a variety of steps need to be taken in order to probe electronic flow. Figure 2.1 describes the general process for exfoliated graphene (see section 2.1.3), the bulk of the devices.



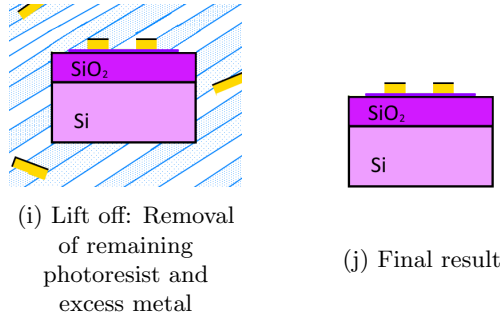


Figure 2.1: Device fabrication process from exfoliated graphene to a FET device.

### 2.1.1 Graphene

Since the realisation of graphene in 2004<sup>[1]</sup>, much research has been focused to finding efficient ways of producing large amounts of graphene<sup>[2]</sup>. Originally, the first samples ever created which have primarily been used for sensitive measurements have been conducted using a method of exfoliation (section 2.1.3). These samples typically exhibit better electronic properties than those produced by other methods. Since 2008/2009, CVD (section 2.1.2) of carbon to create graphene films has provided another prominent method to produce large films for industrial scale applications. In particular, growth of graphene on copper sheets<sup>[3]</sup> has been a reliable way producing these large uniform sheets.

There are other methods not used in this thesis, such as epitaxial growth of graphene via SiC uses heating to boil off silicon atoms to form a layer of graphene on it's surface.

### 2.1.2 Chemical vapour deposition graphene

Graphene can be growth via chemical vapour deposition, resulting in particularly large uniform sheets when grown on copper<sup>[3]</sup>. This is a widely used method of producing readily available graphene. Graphene produced in this fashion needs to be transferred onto an insulating layer of oxide to create a gate, or be gated by using a deposition method. We have used the former, which will introduce some cracks, folding and wrinkling disorder when transferred.

To achieve this, a process<sup>[4]</sup> using poly-methyl methacrylate (PMMA) is used to 'wet transfer' CVD graphene onto a  $\text{SiO}_2$  wafer with pre-deposited Au pads, from a masked e-beam deposition (see section 2.1.6).

Copper grown CVD graphene, covered by PMMA, is placed in an ammonium persulfate solution, dissolving the copper. The remaining graphene and PMMA remains hydrophobic on the surface, and allows substrates to collect the sample beneath. After the transfer is complete, the sample is soaked in PG remover to clean off PMMA. An example device is shown in fig. 2.2.

We seldom used this technique to produce graphene devices due to the area coverage requirement of an oxide as well as the lack of geometric definition.

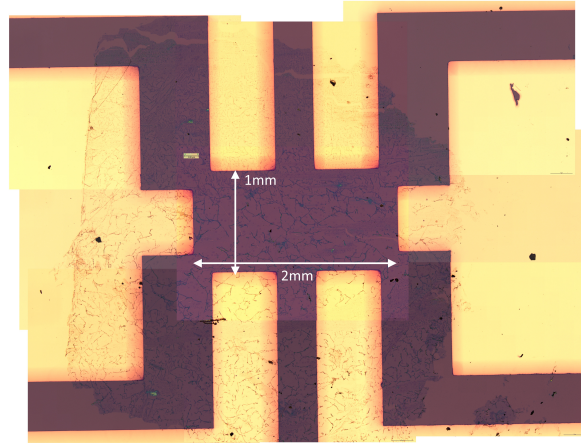


Figure 2.2: CVD graphene grown on Cu transferred onto  $\text{SiO}_2$  and Au pads. The contrast differences due to the autoexposure of the camera software.

### 2.1.3 Exfoliation of graphene

Exfoliation in materials refers to the cleaving thin layers (or leaves) off a larger sample, and acquiring them onto the substrate. We exfoliate graphene onto Si/SiO<sub>2</sub> wafers. Generally exfoliation involves pressing tape/surfaces against a bulk crystal (such as highly orientated pyrolytic graphite (HOPG), Kish graphite, natural graphite, or graphenium). Due to van der Waals interactions, layers of graphite are transferred to the desired surface. By repeated peeling of the same tape, a thin coverage can be obtained and then transferred onto substrates, such as SiO<sub>2</sub>. Exfoliation can take a variety of forms, from Geim's method<sup>[5]</sup>, to directly applying scotch tape to HOPG and then pressing against SiO<sub>2</sub>, before peeling the tape off.

Huang *et al* investigated a reliable method of exfoliation to produce large area and high quality samples<sup>[6]</sup>, which has been widely cited. Tape with graphite flakes is brought into contact with a silicon dioxide wafer, and an annealing process of heating the tape and wafer for 2-5m at  $\sim 100^{\circ}\text{C}$  on a conventional lab hot plate is used. After allowing cooling to room temperature, the tape is removed. They find under optical microscopy that graphene flakes with uniform thickness routinely range from  $\sim 20\mu\text{m}$  to above  $100\mu\text{m}$ . In this context, annealing is expected to increase traction due to the remove of gas molecules trapped between SiO<sub>2</sub> and graphite.

The following steps make up the process of exfoliation we optimised:

1. (Optional) Use a plasma ashing/etcher with an argon/oxygen plasma to the clean surface of SiO<sub>2</sub>. This can increase the adhesion between graphene and the surface by removing organic absorbates<sup>[6]</sup>. Alternatively, clean wafers of Si/SiO<sub>2</sub> in acetone, tilted in an ultrasonic bath for 30s. Repeat the same in isopropanol, before rinsing in ethanol and drying with N<sub>2</sub> gas.
2. Cleave a layer of HOPG graphite by using scotch tape to peel off a thick film.
3. Use a secondary piece of scotch tape to exfoliate a thinner layer off master tape. Ensure good coverage by reattaching a couple times.
4. Attach Si/SiO<sub>2</sub> wafers to graphite covered areas of secondary tape. The SiO<sub>2</sub> face should be contacting the graphite.
5. Attach the tape and wafers firmly to a glass slide, before using a tissue/cotton-bud to press the surface of the tape into the wafer.
6. Place glass slide on a hotplate at  $100^{\circ}\text{C}$  for two minutes, before removing and cooling for two minutes.
7. Slowly peel tape at an acute angle from the glass slide, roughly at 6s per cm over the wafer.

We found success can depend on HOPG crystal, given we tried cleavage using ZYA and ZYB quality crystals and had repeated failure. Changing to a new ZYA crystal provided immediate results using the same process.

After exfoliation, graphene was identified under a 20x microscope lens, raster scanning across wafers to identify any samples big enough. Typically to make a device using photolithography, a sample of graphene required a minimum  $8\mu\text{m}$  in dimensional length to be useful.

### 2.1.4 Lithography

Lithography can be used to create polymer structures that allow the deposition of desired material in 2D geometries. This is used to create electrical contacts onto graphene. This process and the adjustments made for fabricating our devices are described in this section.

Lithography typically consists of three main steps.

1. Spin coating - covering a sample with a uniform layer of polymer, and baking it on.

2. Exposure - The polymer undergoes chemical changes to its properties when exposed to particular wavelengths of light. This differentiates exposed areas to those unexposed.
3. Developer solution - developer solution removes intended areas of photoresist to create structures.

#### 2.1.4.1 Spin coating photoresists

A spin coater is used to deposit thin films of materials. A vacuum holds a sample on the spinner, before drops of photoresist are introduced to the sample, which is then spun over sometime to achieve a uniform thickness of photoresist. Baking on a hotplate follows to set the photoresist layer on the sample.

Photoresists vary in their spinning thickness, but also their exposure rates. Positive photoresists dissolve in particular developer solutions when exposed to light, while negative photoresists dissolve if not exposed to light. We have only used positive photoresists, as we have primarily been creating structures for deposition, and not etching material where you want the bulk of the wafer exposed.

**HMDS & AZ-1512HS** Initially devices were fabricated using the AZ-1512HS polymer, with the additional use of hexamethyldisilazane (HMDS) as an adhesion promoter between  $\text{SiO}_2$  and AZ-1512HS. Devices were spun initially for 10 s at 1000 rpm, before being spun between 2000 and 3000 rpm for 30 s, per resist layer. This leaves a thickness of 1.7  $\mu\text{m}$  to 1.39  $\mu\text{m}$ <sup>[7]</sup>. Devices were then baked at 100 °C for 1 minute.

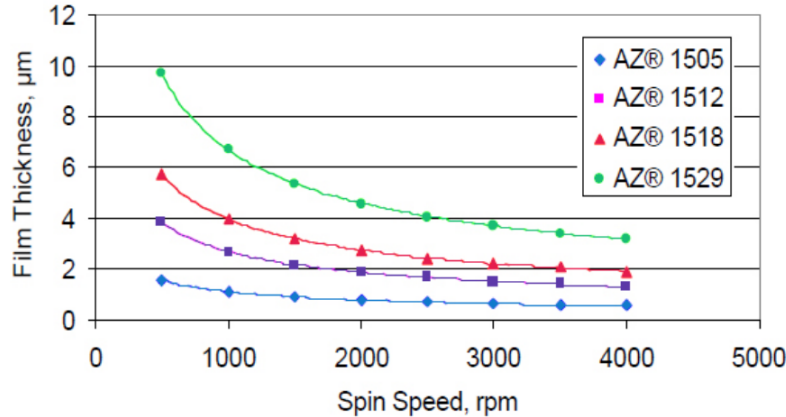


Figure 2.3: Spin curve of AZ-1512HS (Source: EMD Performance Materials<sup>[8]</sup>)

**Skin issues with HMDS** When using HMDS and AZ-1512HS in conjunction, significant amounts of deposition remenants were found on samples as seen in fig. 2.4.

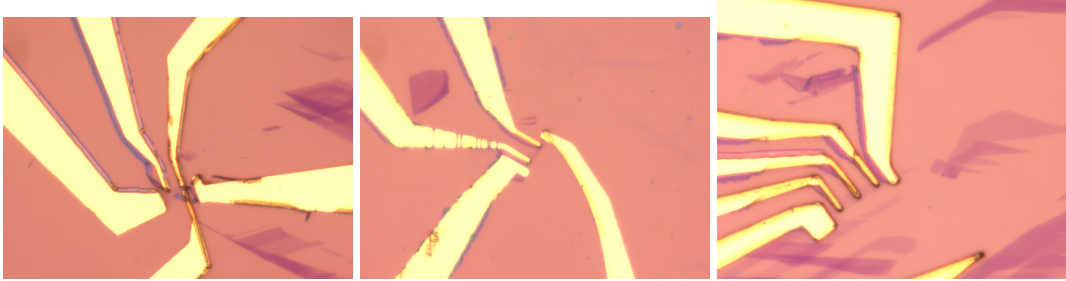


Figure 2.4: Material remnants from lithography. Gold edges exhibit a bluish remnant edge.

This is likely due to metal deposition (i.e. Chromium, see section 2.1.6) forming layers on the sides of lithography wells, as the skins have very similar geometry to that of either the wells or the edges. The spinning speeds give resist heights (i.e. the well edge heights) roughly the same as feature width ( $\approx 1\mu\text{m}$  minimum), matching the observed result.

Ultrasonication (see section 2.1.7.1) can be used to attempt to remove edges after lift off, however there is risk of damaging samples of graphene.

**LOR-1A & AZ-1512HS** The issue with a single layer photoresist processes, outlined above, is that well edges allow deposited materials to adhere, leaving 'skins'. One way to prevent this from happening is to use a multilayer process. Two resist layers are spun onto the sample, with the bottom film being more sensitive to the lithography process than the top (i.e., develops faster, or is more sensitive to exposure). When developed, the bottom layer *undercuts* the top layer, stopping adhesion to edges of the well when material is deposited. This process is depicted in fig. 2.5.

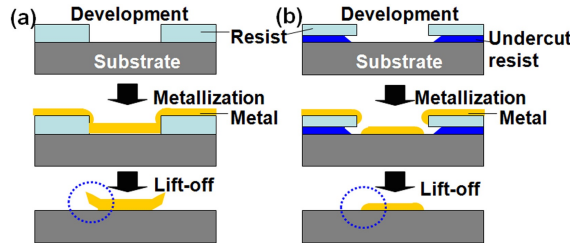


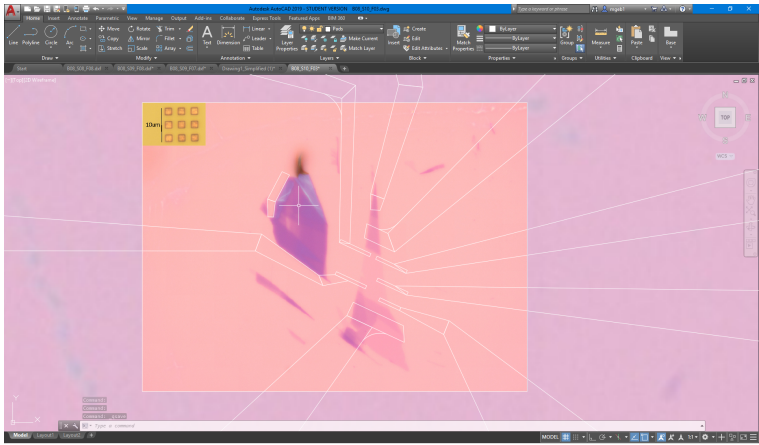
Figure 2.5: Bilayer lithography process (Source: Park *et al*<sup>[9]</sup>)

LOR-1A is an actinic lift off resist, responding to UV light from 240 nm to 290 nm<sup>[10]</sup>. When the resist films are exposed to the developer, LOR-1A is removed below an overhanging AZ1512-HS layer due to additional development, leaving the desired undercut effect.

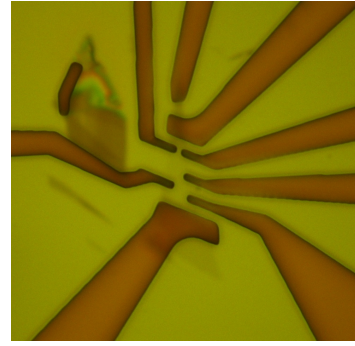
#### 2.1.4.2 Exposure

After spinning, a mask writer tool is used to expose the wafer and resist films to UV light. A mask writer is composed of a mask, or a DMD (digital micro-mirror device) which allows filtering of pixel like squares, based on an input image. Actinic reactions occur from the UV light with the photoresist, forming desired pad structures in the resist. Prepared CAD files are used to generate masks used by the DMD as seen in fig. 2.6.

An important parameter in the mask writing process is the exposure time, which affects the ability to develop fine structures. By using an array of different exposure times (fig. 2.7), the optimal feature result was found for a typical developing time.



(a) DMD masks created using Autocad™. Additional structures are created to help position the mask when using a 20x lens, as graphene can be difficult to see in a mask writer tool.



(b) Photolithography structure from mask writing and development.

Figure 2.6: Photolithography mask writing

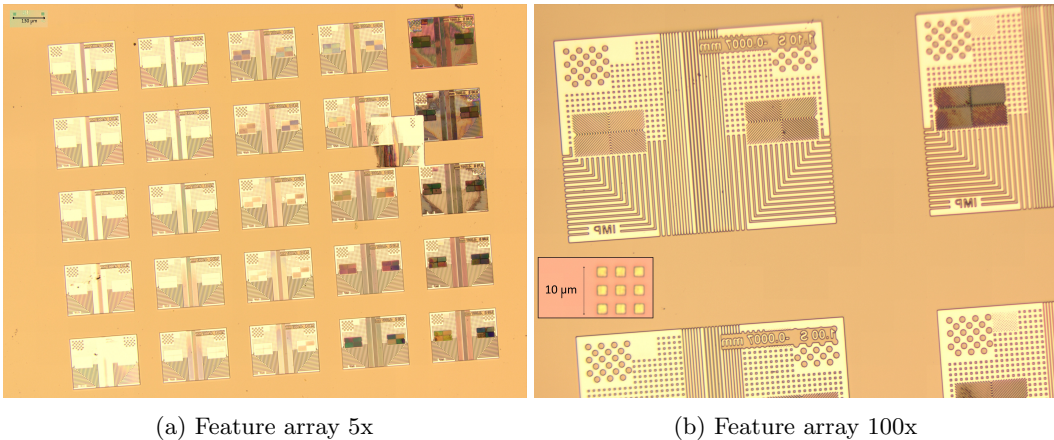


Figure 2.7: Developing an exposure array on  $\text{SiO}_2$

#### 2.1.4.3 Developers

Developers are used to dissolve exposed / unexposed areas of photoresist films. We use AZ-726 in conjunction with AZ-1512HS. Using a development time complementary to the exposure time is important to not overdevelop features, as material in proximity to exposed areas is at risk of some structural damage, and developers continue to react with the remaining structure over time.

#### 2.1.4.4 Contact pad dimensions

To make contacts large enough to connect probestation probes to (see section 2.2.2), Au pads were created usually with a minimum dimension of  $400\mu\text{m}$  width, and a larger length dimension. This meant that wirebonding was not necessary for small contacts, which saved one step of the measurement process, although PCB boards had been designed with wirebonding in mind (see section 2.1.9).

### 2.1.5 UV Ozone surface preparation

Large resistances can occur when trying to make contact with graphene. This can be for a variety of reasons. Resist residues between the deposited pads and graphene can be insulating, perhaps non-metallic bonding occurs between deposited metals and graphene, or the oxidisation of metals being deposited (i.e., chromium oxide) could occur.

Several studies by Li *et al.*<sup>[11]</sup> and Nath *et al.*<sup>[12;13]</sup> have shown the ability to reduce contact resistance of graphene by using UV ozone treatment, to less than  $200\ \Omega$ , a small contact resistance.

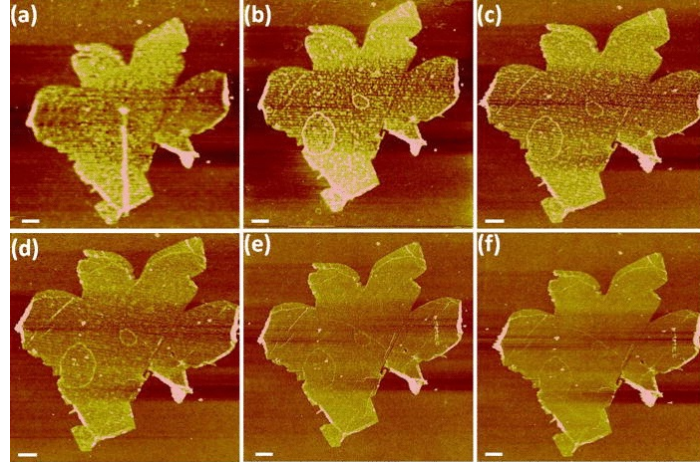


Figure 2.8: Cleaning of graphene using UV Ozone (Source: Li *et al.*<sup>[11]</sup>)

(a) Before transfer (b) After photolithography (c)→(f) UVO treatment for 5, 10, 16, 22min, respectively. Scale bar:  $1\mu\text{m}$ .

UV Ozone treatment refers to the use of UV light to generate photochemical reactions on sample surfaces. 185nm light is used to generate ozone  $\text{O}_3$  from bonding molecular ( $\text{O}_2$ ) oxygen, while 254nm light is used to dissociate ozone to molecular and singlet oxygen ( $\text{O}_1$ ), the latter of which is reactive with substrate surfaces. Increasing stage temperature also will increase the etching rate that occurs. UV Ozone is used in this context to clean the graphene exposed in our developed wells, as seen in fig. 2.8.

To determine an appropriate etching time for the particular tool used, two wafers with grapehe flakes at times of 5m and 15m were cleaned using UV Ozone. The 15m devices were etched away completely, however the 5m device provided the first low resistance contact observed, after many iterations of devices.

### 2.1.6 Deposition

Once a designed structure is built to make contacts with graphene and cleaned using UV Ozone, material can now be deposited onto the device. There are many different methods, including sputtering and thermal evaporation, however electron beam evaporation (fig. 2.9) was used for these devices, due to its uniformity, control of deposition rate, and the availability of various material crucibles.

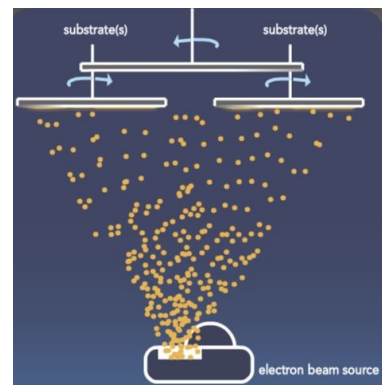


Figure 2.9: E-beam Evaporation  
(Source:<sup>[14]</sup>)

50nm of Au (Gold) was originally deposited with a Cr (Chromium) adhesion layer of 5nm to promote contact to SiO<sub>2</sub>, however issues with metallic contact to graphene arose. In case of chromium oxidisation during deposition, creating an insulating layer to graphene, a thinner layer (2nm) of chromium was instead deposited. This is reasonable as pinhole effects resulting from a thin deposited Cr layer do not affect bulk transport.

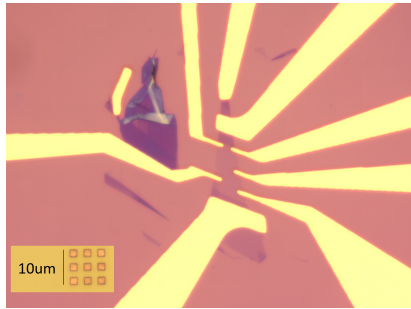


Figure 2.10: Cr/Gold/Cr/SiO<sub>2</sub> contacts.

### 2.1.6.1 Oxide Protection

In using metal liquids to cover devices with oxides, the gold reacted strongly to the liquid metallic environment, destroying pre-established pads. This is further described in chapter 5, however the result was to use additional layers, another layer of Cr 2nm and a layer of SiO<sub>2</sub> 20nm. These additional layers do not prevent contact through contact probes and provide insulation from the bulk of metal liquid reactions.

### 2.1.7 Lift-off

To remove the remaining gold covered photoresist on the substrate, a solvent called PG remover is used to emerse samples at 80 °C. Using a pipette to generate soft fluid flow around the device, the excess gold is slowly removed.

### 2.1.7.1 Ultrasonication

After lift off, the presence of skin remnants (described in section 2.1.4.1) could sometimes be cleaned off through the use of ultrasonication (fig. 2.12), however this had a large risk of damaging the graphene, seen in fig. 2.13.

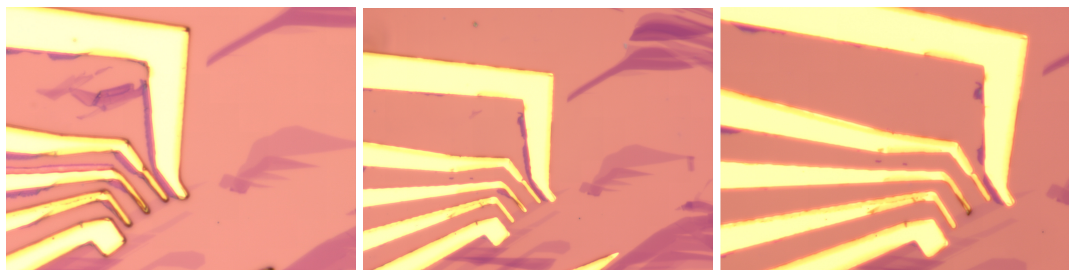


Figure 2.11: PG Remover liftoff.

Figure 2.12: Ultrasonication used to remove material remnants from lithography.

Note the movement or loss of gold material on the middle probes.

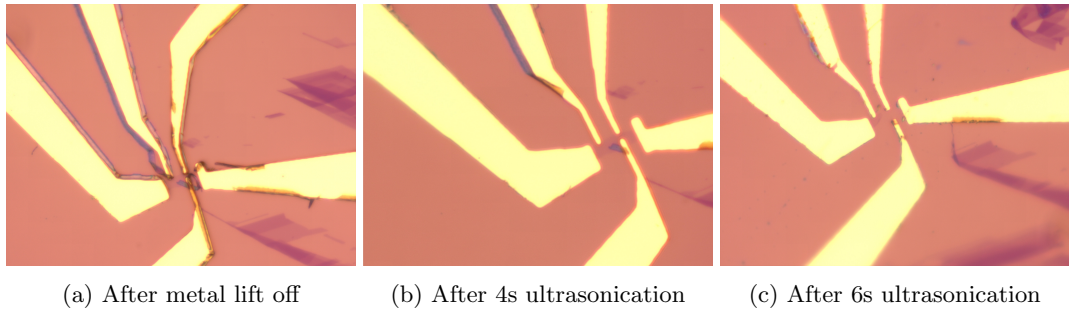


Figure 2.13: Ultrasonication that has broken graphene sample.

### 2.1.8 Argon/Hydrogen Annealing

Many researchers who have produced electronic devices from graphene use an Argon/Hydrogen annealing process to clean their samples from polymer residues remaining from transfer or lithography processes. [15;16;17;18]

We use a process of heating for 30 minutes to 340 °C, annealing with flow rates of 400 sccm Ar / 200 sccm H for 2 hours, before naturally cooling back to ambient temperature.

### 2.1.9 PCB board mounting



Figure 2.14: Ag/H annealing of exfoliated graphene devices



Figure 2.15: PCB for mounting wafers to connect backgates and wirebond pads of device.

PCB boards were designed for mounting small 1 cm<sup>2</sup> Si—SiO<sub>2</sub> wafers. Wafers are mounted using a conductive silver epoxy (CircuitWorks Conductive Epoxy) from Chemtronics. PCB's were produced through PCBway.com, using a singe layer design with immersion gold surface finishing. Unfortunately the FR4-TG (flame retardant glass transition temperature) was selected at 130-140, which means these boards cannot withstand temperatures above 140 °C. PCBway also offer a 180 TG option, which would be used in the future.

These PCB boards provide pads to connect probes to the backgated Si. Additionally, to avoid scratching of lithography pads, extra pads surround the mounting point to wirebond connections to, and then place probes onto.

PCB Designs using Autocad Eagle software can be found at [github.com/mattgebert/eaglecircuits](https://github.com/mattgebert/eaglecircuits).

### 2.1.10 Oxide stamping

Zavabeti *et al*'s<sup>[19]</sup> work on thin oxides synthesised by liquid metal introduces two methods to create such oxides. The first involves the exfoliation of oxide layers from the surface of metal droplets, and the second involves the suspension of oxide layers in water, created by injecting gas through the metal liquid. This section will only describe the former in detail, which is used in this project. Refer to chapter 5 for further optimisation and exploration of the liquid metal technique.

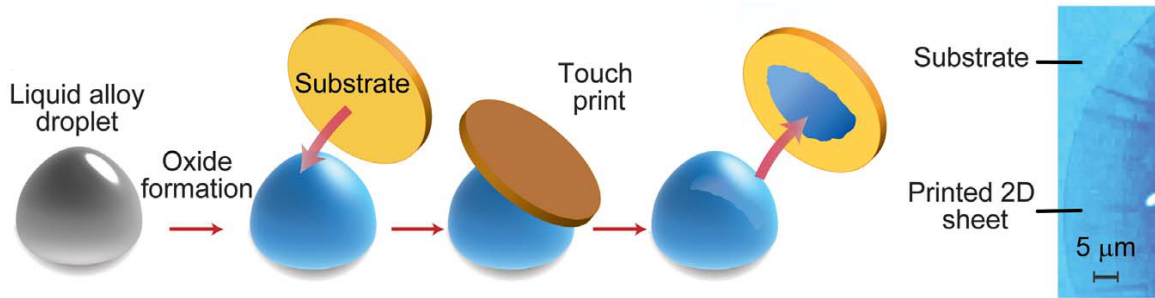


Figure 2.16: Process of liquid metal oxide exfoliation (source: Zavabeti *et al*<sup>[19]</sup>)

A eutectic gallium melt is made by combining elements such as gallium, indium and tin. At room temperature these alloys are metallic liquids, and form atomically thin oxides on their surfaces. Because the formation of oxides change the Gibbs free energy of the system, those that provide the greatest reduction dominate the surface<sup>[19]</sup>. After the melt is formed and exposed to oxygen for some time, the oxide is isolated by a van der Waals exfoliation technique, touching the liquid metal droplet to the solid substrate, as seen in fig. 2.16.

For the synthesis of  $\text{AlO}_3$ , aluminium pieces are cleaned using a tissue, before being cut up into a few mm long segments. After heating a gallium based melt into a liquid inside a glovebox with roughly 0.2-0.3% oxygen, the gallium and aluminium are ground together using a mortar and pestle. After this, some time is taken for the oxide to form on the surface of the liquid metal (put on glass slides for accessibility). Substrates are touched lightly, and should be able to be removed from the liquid metal droplet without adhering the liquid, but obtaining a thin oxide layer.

## 2.2 Measurement techniques

To measure the electrical properties of graphene devices (such as those detailed in section 2.1), particular equipment and methods are employed to observe relevant properties.

### 2.2.1 4 probe measurements

4 probe measurements, also known as Kelvin sensing, utilise four probes to make a more accurate measurement than regular two probe measurements.

Conventional multimeters use a probing voltage with a galvanometer to detect a current running through a sample (in this case, graphene). Based off the detected current, a measurement can be made of the resistance for the known voltage. Because exfoliated graphene can have very small channel widths, it is very sensitiviy to large currents and consequently makes using a multimeter dangerous. Using a multimeter would be fine however, for large area CVD graphene.

One advantage of using a 4 probe measurement is that you can use a current-limiting resistance, which has a much larger resistance than your sample ( $> 100\times$ ). This allows control of the current running through your sample, ensuring safe limits, and means the resistance of your sample will affect

the current flow to less than 1%. By observing the voltage difference across the sample, a resistance can be inferred from the flowing current. Typical exfoliated graphene devices used in this project have a measured resistance on the order of  $\approx 5 \text{ K}\Omega$  (eq. (2.1)).

However, the most significant advantage of using a 4 probe measurement is the ability to avoid including contact resistance, created by the junctions between contact pads and the material of interest (graphene). This is illustrated in fig. 2.17. A 4 probe measurement uses a voltage difference measured by probes at different points on the sample material, thereby avoiding any contact resistance included in series, and sampling the voltage along the sample. An example resistance calculation is shown in eq. (2.1).

$$R = \frac{V_{b-a}}{I} = \frac{V_{b-a}}{(V_{\text{source}} - V_{\text{GND}}) / R_{\text{limit}}} = \frac{5 \times 10^{-3} \text{ V}}{1 \text{ V}/10^6 \Omega} = 5 \text{ K}\Omega \quad (2.1)$$

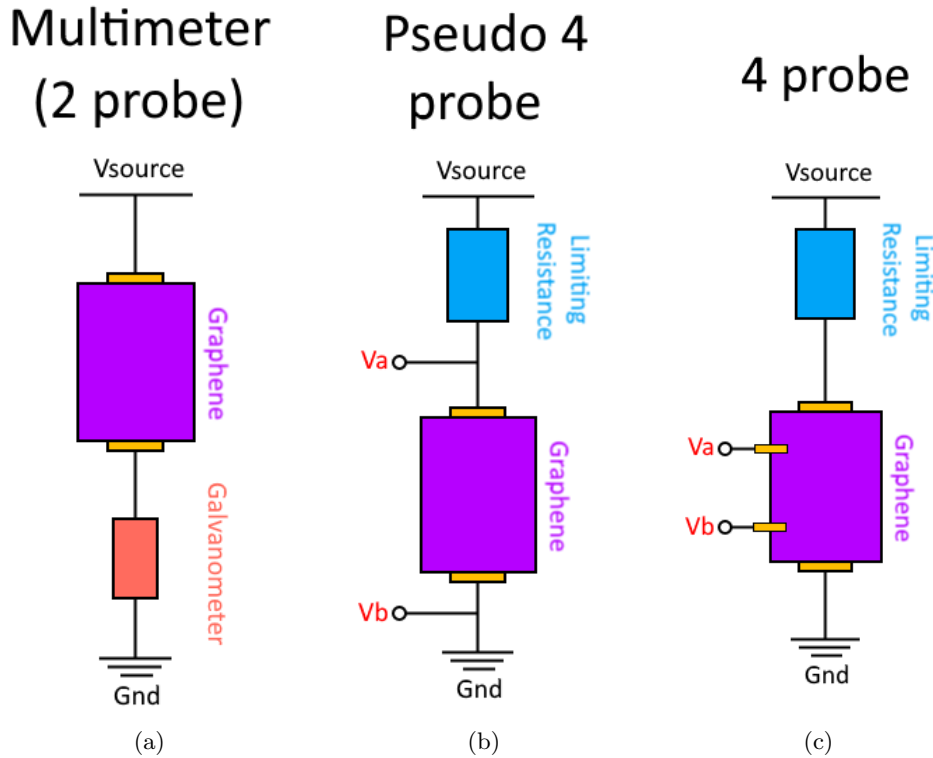


Figure 2.17: Schematics of resistance measurements. (a) A multimeter provides little control over the current through the sample, and measures any resistance formed between the gold contacts and the graphene. (b) A pseudo 4 probe measurement uses a voltage difference across the device to calculate its resistance, inclusive of the series resistance due to the gold contacts. (c) A 4 probe measurement uses a voltage difference measured by probes at different points on the sample material, thereby avoiding any contact resistance included in series, and sampling the voltage along the sample.

### 2.2.1.1 Sourcemeters

A sourcemeter has the ability to source and measure a stable DC voltage or current. They provide precision, low noise and stability. We use Keithley 2400 SourceMeters<sup>[20]</sup> which source voltage from

$5\mu\text{V}$  to  $210\text{V}$ , and current from  $50\text{pA}$  to  $1.05\text{A}$ , and can deliver 520 readings per second at  $5\frac{1}{2}$  digits (ie, 199999).

A source meter is used in 4 probe measurements to apply a constant, controllable gate voltage to the Si as directed in fig. 2.18. Changing the potential of Si under  $\text{SiO}_2$  changes the charged carrier density (electrons, holes) on graphene by using the  $\text{SiO}_2$  as a capacitor dielectric. This allows the measurement of the resistivity of graphene as a function of carrier density.

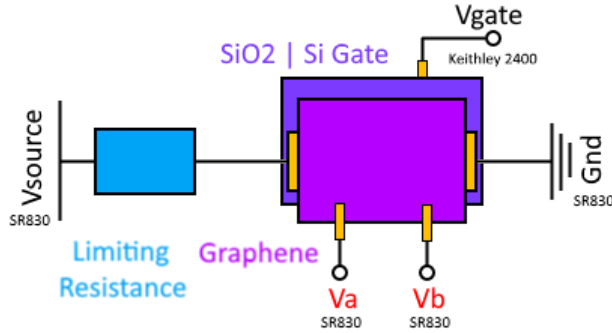


Figure 2.18: Instrumentation connections to a gated graphene FET, using a Keithley 2400 SourceMeter and a SR830 Lock-In Amplifier.

### 2.2.1.2 Lock-in amplifiers

A lock in amplifier is used to measure very small AC signals. This project used a Stanford Research 830 Lock-in amplifier<sup>[21]</sup>, which uses a significant amount of digital digital processing (DSP) for it's functionality. It operates on the principles of signal mixing - multiplying a input signal ( $f_s$ ) that is expected at a particular frequency by a reference signal ( $f_r$ ). This mixing generates a DC signal whose amplitude can be measured, directly inferring a signal strength. An example calculation of mixing is shown below in eq. (2.3).

$$f_s \otimes f_r = \cos(\omega_s t + \phi) \otimes \cos(\omega_r t) \quad (2.2)$$

$$\begin{aligned} &= [\cos(\omega_s t) \cos(\phi) - \sin(\omega_s t) \sin(\phi)] \otimes \cos(\omega_r t) \\ &= \cos(\phi) \frac{1}{2} [\cos((\omega_s + \omega_r)t) + \cos((\omega_s - i\omega_r)t)] \\ &\quad - \sin(\phi) \frac{1}{2} [\sin((\omega_s + \omega_r)t) + \sin((\omega_s - \omega_r)t)] \end{aligned} \quad (2.3)$$

When the two frequencies  $\omega_s$  and  $\omega_r$  are close, then the sinsoidal components  $\omega_s - \omega_r$  form a DC component, while high frequency compliment can be filtered. Only noise close to the signal frequency will be picked up in the filtering, and will only result in low frequency AC output.

The lock in amplifier uses a phase locked loop to generate a reference signal, which is a particular control circuit. The lock in amplifier can either run independently, generating it's own output, or can be locked to an external signal. We use the former in our measurements, to pass a slow 17Hz signal of amplitude  $1\text{V}_{rms}$  through graphene devices.

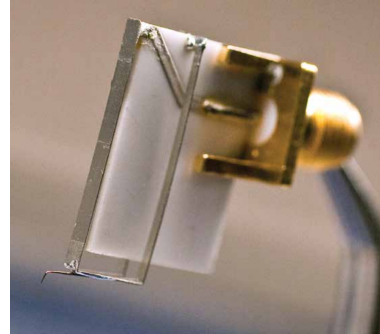
A voltage difference is calculated between probes on graphene by the lock in amplifier and outputted. The real component of the voltage difference and the complex phase are recorded - we expect the bulk transport in graphene to be resistive, and a phase is measured to confirm that as we measure.

## 2.2.2 Probe station

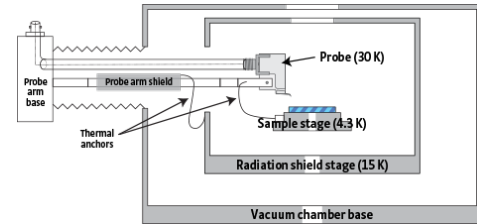
A LakeShore cryogenic probestation (fig. 2.19) was used to load sample wafers and measure their electronic properties under controlled conditions. In particular, we will touch on temperature control, vacuum ability, and the risk of static discharge.



(a) LakeShore probestation, with coolant inlet, 6 probe arms, vacuum seal and microscope camera.



(b) Tungsten spring probes, 25  $\mu\text{m}$  radius tip



(c) Schematic diagram of probestation, showing connections from probe arms to sample stage and temperature limits of elements

Figure 2.19: LakeShore probestation

### 2.2.2.1 Vacuum

A roughing pump is used in conjunction with a turbo pump to create pressures of  $1.5 \times 10^{-2}$  mBar and  $5 \times 10^{-5}$  mBar (turbo at 1.35 kHz operational frequency). This pumping removes any trapped oxygen and contamination of gasses that might condense onto our sample of graphene at low temperature.

### 2.2.2.2 Temperature control

Temperature is controlled by a combination of heating and cooling power. The metallic inlet protruding from under the main stage in fig. 2.19 allows the flow of liquid nitrogen/helium through the sample stage to cool down the sample. This process is illustrated in fig. 2.20.

Heating is provided via a 50W calibrated silicon diode. Thermocouples with high accuracy allow the ability to control the heating power to stabilise to a setpoint temperature, with small fluctuation. This is achieved by the use of a PID controller system, where

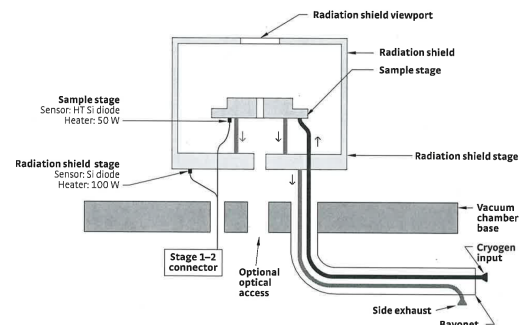


Figure 2.20: Probstation refrigerator

the measured temperature difference from a setpoint is used to control the diode power. By using the proportional, integral and differential gains, rapid and stable responses to shifts in desired temperature are controlled.

- Proportional gain adds some power based on the difference from the desired solution.
- Integral gain ramps the power over time, based off long term difference. This prevents offsets from a final setpoint.
- Differential gain only considers the changing response. It smoothens trajectory of PI controller, reducing overshoot and stabilising levels faster.

### 2.2.2.3 Static Discharge

Care needs to be taken when using the probestation with small graphene samples. Static discharge can cause large potential differences across graphene, consequently burning the sample by a high current. Discharge can be protected against by taking some precautions below.

BNC cables employ a coaxial (ground and signal) wire configuration, and are used to connect to the probestation. This ensures the probestation shield is grounded, the same as the instrument ground. This protects the device from any external static buildup. If the probes are then grounded, they are at the same potential as the shield.

Additionally, when a measurement was not taking place, BNC connections to the device were grounded using  $50\Omega$  terminators, connected via T terminals to avoid floating connections and minimising static while connecting terminators. This meant that any external charge would have a low resistance current path to flow, thereby protecting the sample.

Static straps were also worn and connected to the instrument ground to ensure no clothing item would build up static on an individual.

### 2.2.2.4 Probes

A combination of regular and flexible tungsten probes are used in the probestation to make electrical connections to samples. When touching probes down, the respective BNC was connected to a  $10 M\Omega$  resistance terminator. Rather than protecting from external static, this was in case the sample (sometimes doped) was resting at a potential other than ground, and had free charge to discharge. A high resistance terminator slows this current, before allowing the connection of an appropriate ground.

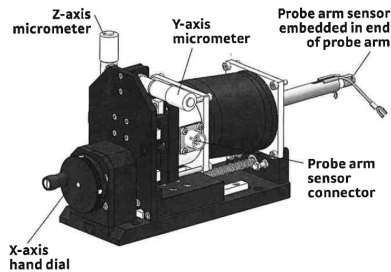


Figure 2.21: Probestation micro-manipulated stages

## Chapter 3

# Characterisation of graphene

### 3.1 Raman spectroscopy

Raman spectroscopy uses monochromatic light to observe scattering processes on an incident material. Four fundamental processes describe the scattering behaviour: IR absorption, Rayleigh scattering, or (anti) Stokes Raman scattering. The latter (two) processes scatter light, by interactions with phonons or other excitations. This changes the incident light's momentum and energy, resulting in a frequency change. By measuring the returning light and its spectral distribution, information is gained of the vibrational modes within the material. Devices such as charged coupled devices (using MOS or CMOS transistors) allow for sensitive measurements of the light. Photons that are scattered with the same initial energy (Rayleigh Scattering) are filtered.

#### 3.1.1 Raman in graphite

Historically, the Raman profile for graphite is well established<sup>[22]</sup>. Since the invention of the laser to make sensitive, monochromatic measurements, Raman spectroscopy conducted on graphite in the 1970's had yielded a distinct profile of the phonons existing within materials<sup>[23;24;25]</sup>. At the beginning of the 80's Vidano's group profiled graphite samples across multiple Raman wavelengths, properly profiling different peaks<sup>[22]</sup>.

Peaks are listed as follows:

- **G** ( $\approx 1580/\text{cm}$ ) The active  $2E_{2g}$  mode of the hexagonal symmetry group. This traditionally has the highest peak intensity in graphite, and is doubly degenerate.
- **2D** ( $\approx 2700/\text{cm}$ ) Higher order scattering, and overtone of D. Second highest peak in graphite. Relabelled as the 2D peak by Ferrari, originally written as G' peak.
- **D** ( $\approx 1360/\text{cm}$ ) Attributed to edge modes (ie zone boundaries) that appear from relaxed wavevector selection rules.
- **D'** ( $\approx 1620/\text{cm}$ ) Splitting from degenerate  $E_{2g}$  due to disorder.
- **D''** ( $\approx 2950/\text{cm}$ ) Higher order scattering.

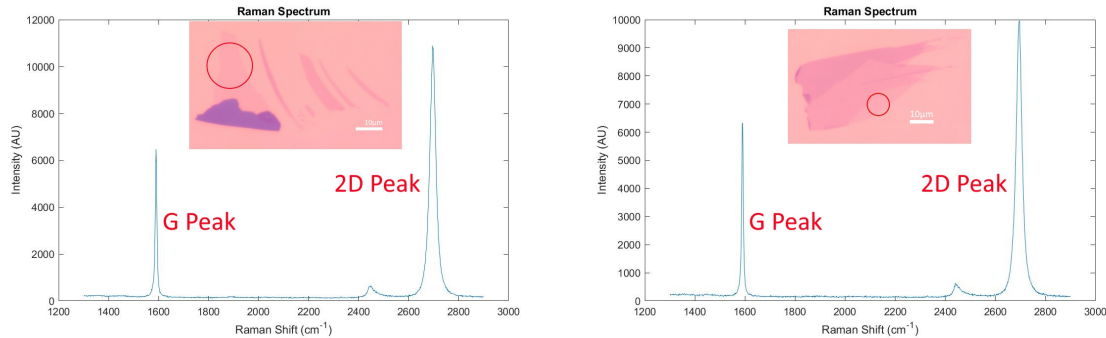
In graphite, the G peak is normally dominant and the 2D peak is split into at least two components at 1/2 and 1/4 amplitudes of the G peak.

#### 3.1.2 Raman in graphene

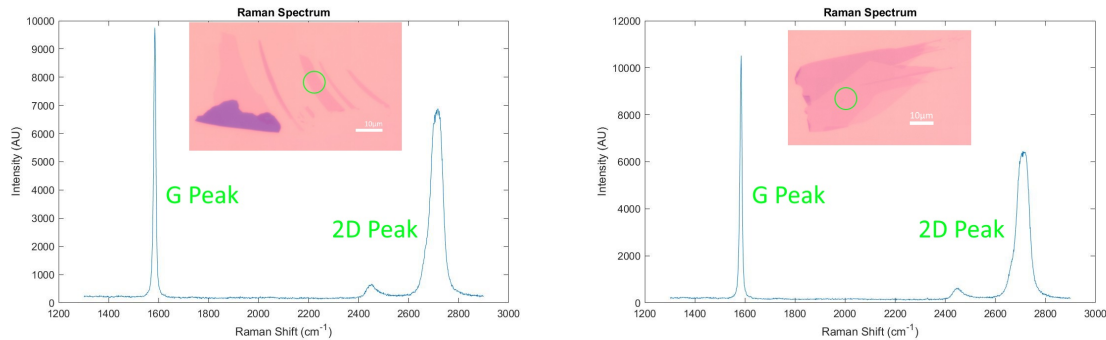
Differing layer numbers of graphene produce unique Raman signals<sup>[26;27]</sup>. This variance in the amplitude and central frequency of maxima. The signals are unique because the vibrational properties of monolayer, bilayer and multilayer are distinct. Ferrari *et al.* observed that Raman is a useful tool for distinguishing between these layers.

Two particular characteristics are useful for characterising layers. Firstly the amplitude of the 2D peak is roughly on the order of 2x that of the G peak in graphene. This ratio drops as the number of layers increases. Only the single layer and bilayer peaks are easily distinct from higher numbers of layers, which are somewhat indistinguishable.

This characteristic is clear in the data we've acquired of numerous graphene samples, and shown below in fig. 3.1.



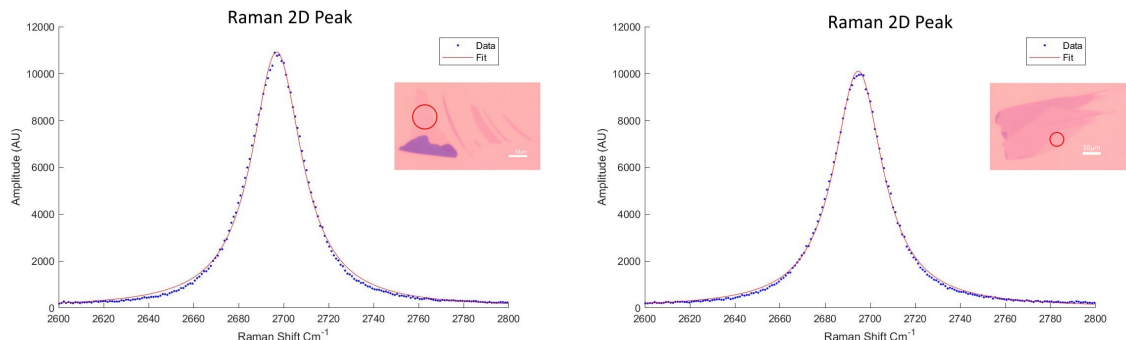
(a) Graphene Raman spectrum.



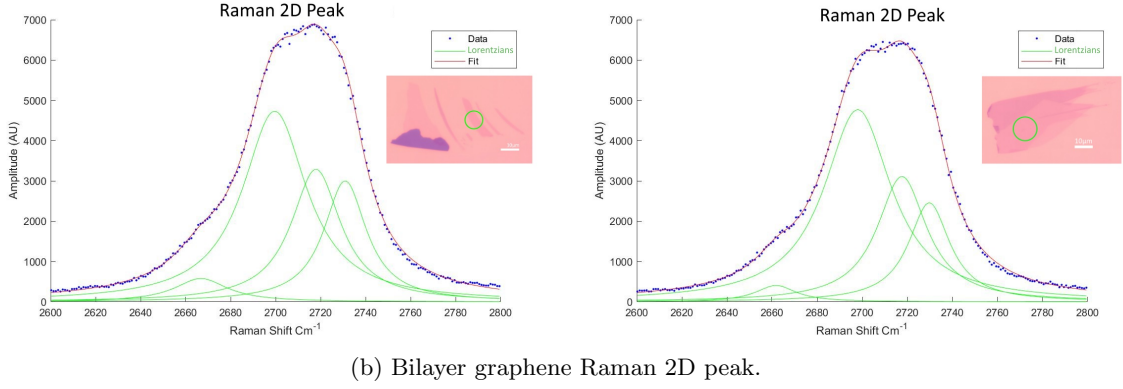
(b) Bilayer graphene Raman spectrum.

Figure 3.1: Ratio of G to 2D Peaks in various levels of graphene

Secondly, the 2D peak slowly shifts right and broadens as layers increase. This is distinguishable between a single layer, two layers and multiple layers. For a single layer, the peak fits very well to a single resonance lorentzian. For two layers, 4 lorentz peaks are used to fit the broader 2D resonance.



(a) Graphene Raman 2D peak.



(b) Bilayer graphene Raman 2D peak.

Figure 3.2: Raman 2D fitting of graphene and bilayer

The theoretical picture is quite intuitive for the broadening of the 2D peak seen in fig. 3.2. Because the 2D peak relates to disorder, and not directly a mode of geometric structure of graphene, it is coupled to the electronic structure (see fig. 3.3). A single layer of graphene has dirac points and allows single transitions in the momentum/energy profile. A bilayer of graphene instead has an extra two bands, allowing a possibility of 4 slightly different transitions near the same energy/momentum profile, contributing to the broadness seen in the Raman spectrum.

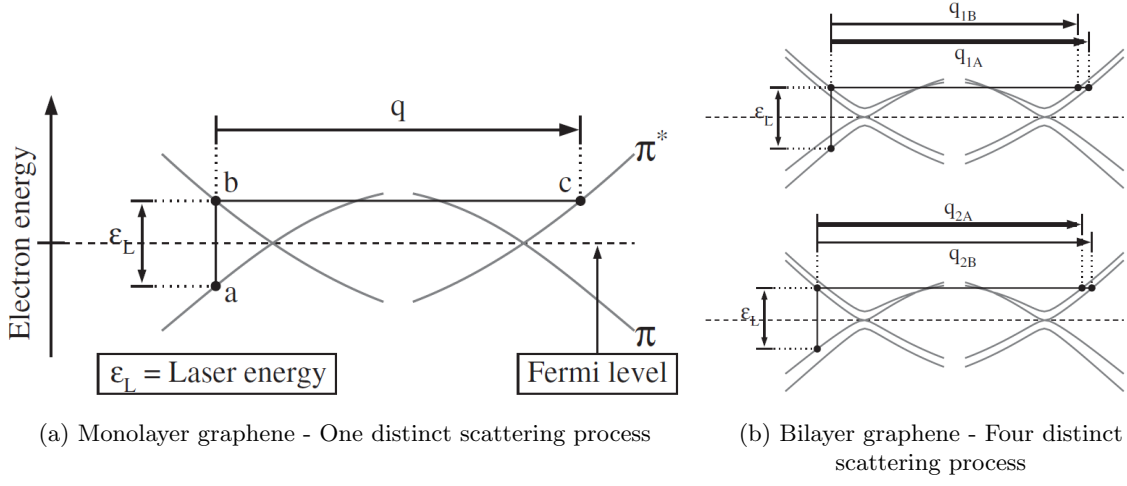


Figure 3.3: Raman scattering processes in graphene and bilayer graphene, coupled to the electronic structure. Each transition results in a unique change of momentum and energy.  
(Source: Ferrari *et al.* [26])

## 3.2 Optical microscopy

Under a microscope, graphene can be optically observed on particular substrates. Blake *et al.* has studied the optimal wavelengths of which to observe graphene, based on the oxide thickness ( $\text{SiO}_2$ )<sup>[28]</sup>. We use 285 nm  $\text{SiO}_2$  on top of Si to make graphene most visible in the green spectrum, most sensitive to the human eye for optical detection (see fig. 3.4). A consequence is that monolayer graphene can be optically identified without the need for more other measurements such as Raman or atomic force microscopy<sup>[29;30]</sup>.

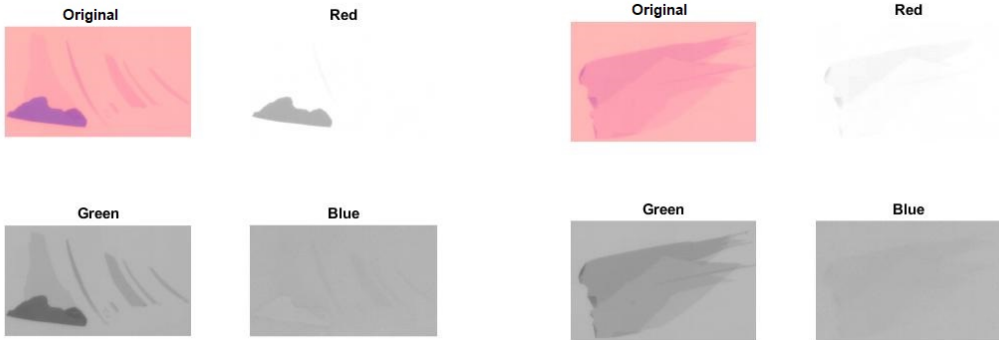


Figure 3.4: RGB decomposition of optical images of graphene on 285nm SiO<sub>2</sub>. Most contrast for single or few layers of graphene comes from the green component as desired.

### 3.2.1 Contrast imaging

Graphene has an opacity related to the fine structure constant. It has 2.3% absorbtion, passing  $\approx 97.7\%$  of the light incident on it. This quantity is actually the fine structure constant, physically defined by fundamental quantities<sup>[31]</sup>. Fundamentally the fine structure constant describes the electromagnetic interaction strength of particles. It is one of the few phenomena in condensed matter physics that doesn't depend on material parameters, and is pretty spectacular (excuse the optical pun) to consider.

Graphene exhibits a universal electrical conductance minimum of  $\approx 4(e^2/h)$ , and as a result<sup>[32]</sup> the optical conductance is also expected to have a fundamental value, behaving independent of frequency (to a broad range of photon energies). This is due to the linearity of the electronic band structure around the dirac points, which phonons interact with.

$$\alpha = \frac{\pi e^2}{\hbar c} \approx \frac{1}{137} \quad (3.1)$$

$$\pi\alpha \approx 2.3\% \quad (3.2)$$

We can use this property of graphene's optical transmittance to perform contrast imaging of graphene, identifying single layers from the contrast between the substrate beneath and the flake of interest.<sup>[29;30;33]</sup>

If light passes from a light source through the graphene, reflects from the SiO<sub>2</sub>, passes back through the graphene then we expect approximately 5% absorbtion to affect our contrast change. We calculate a contrast image by using the green pixel value (0, 1) of each square ( $G$ ) and taking the difference from the background mode ( $G_0$ )<sup>[33;30]</sup>. Dividing by the background mode gives a percentage change.

$$C = \frac{G - G_0}{G_0} \quad (3.3)$$

This formula takes a  $G$  colourvalue representing the background contrast, and observes the percentage change when layers of graphene are on top of it. This percentage absorbtion should roughly match the expected 2.33% per transmission through graphene, as the pixel value approaches black (value  $G = 0$ ).

Figure 3.5 and fig. 3.6 both clearly indicate peaks for single layers near 6% contrast, and multiples of that for larger layers. This is a little higher than expected, but given RGB capture is 0-255, the uncertainty in pixel capture is roughly  $1/255 \approx 0.4\%$  making this deviation reasonable.

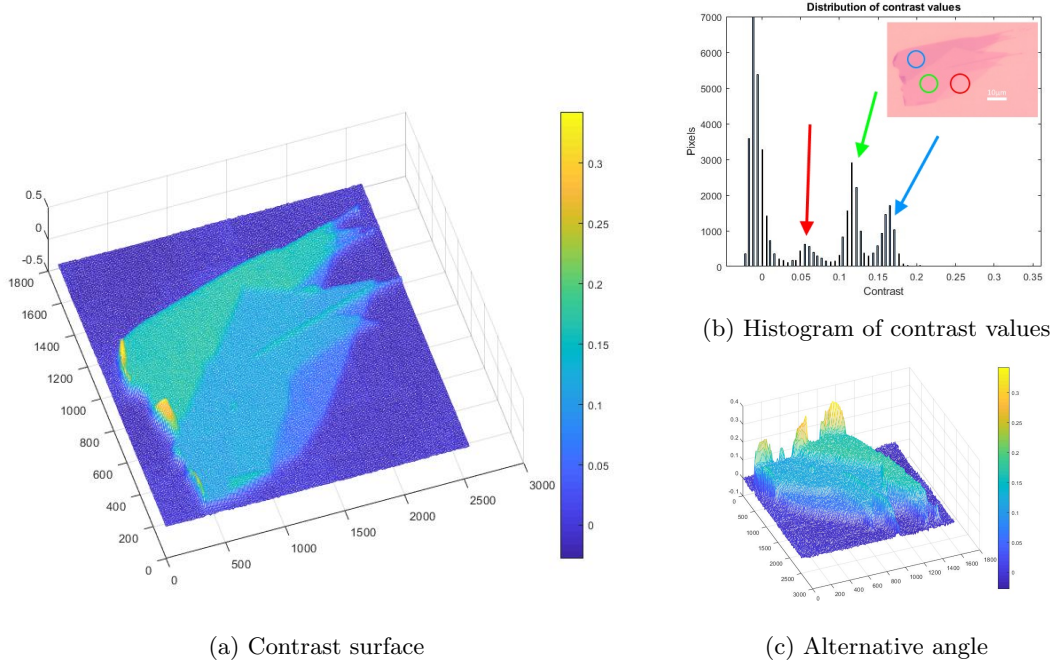


Figure 3.5: Contrast imaging of sample 1.

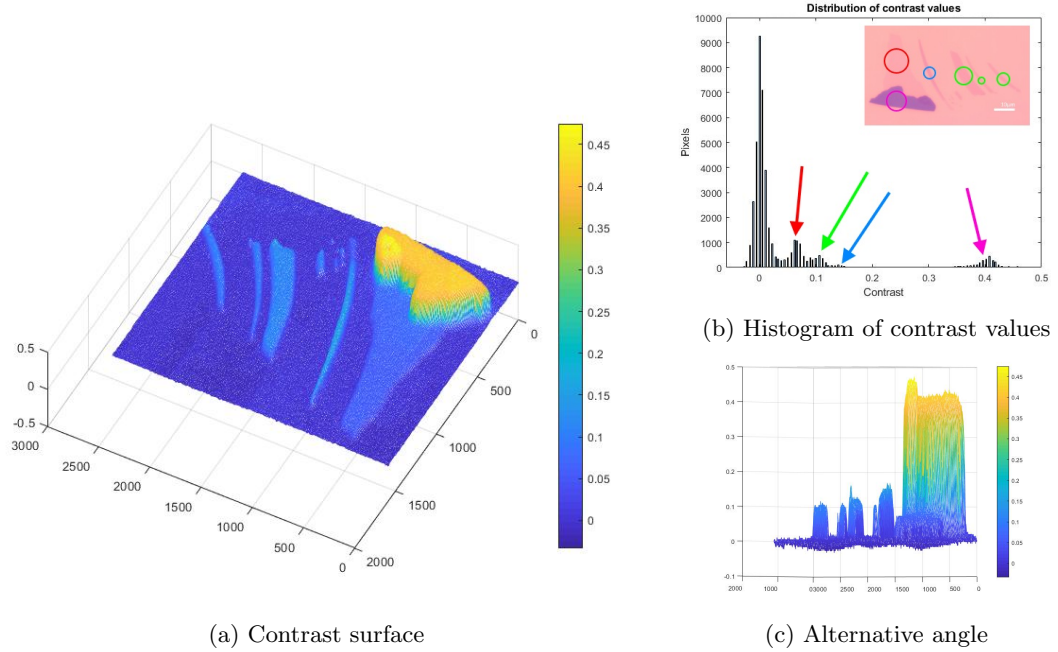


Figure 3.6: Contrast imaging of sample 2.

## Chapter 4

# Electrical measurements of pristine graphene

### 4.1 CVD

### 4.2 Exfoliated

$$C_{\text{flake}} = \frac{G_{\text{SiO}_2} - G_{\text{flake}}}{G_{\text{SiO}_2}} \quad (4.1)$$

$$\partial R = \frac{\rho}{w} \partial L \quad (4.2)$$

$$R = \frac{V}{I} = \frac{V_a - V_b}{I_{in}} \quad (4.3)$$

$$\sigma = \sqrt{(N^* e \mu)^2 + \left( \rho_S + \frac{1}{N e \mu} \right)^{-2}} \quad (4.4)$$

$$N = \frac{C_g}{e} |V - V_G| \quad (4.5)$$

$$\rho[V_g, T] = \rho_0[V_g] + \rho_A[T] + \rho_B[Vg, T] \quad (4.6)$$

$$\rho_A[T] = \left( \frac{h}{e^2} \right) \frac{\pi 2 D a^2 k_B T}{2 h^2 \rho_S V_s^2 V_F^2} \quad (4.7)$$

$$\rho_B[V_G, T] = B \frac{h}{e^2} V_G^{-\alpha_1} \left( \frac{1}{\exp[(0.059 \text{ eV})/k_B T] - 1} + \frac{6.5}{\exp[(0.115 \text{ eV})/k_B T] - 1} \right) \quad (4.8)$$

#### 4.2.1 hBN transfer

# Chapter 5

## Thin oxides

### 5.1 Printing

5.1.1  $\text{Al}_2\text{O}_3$

5.1.2  $\text{SnO}$

5.1.3  $\text{Bi}_2\text{O}_3$

### 5.2 Smearing

5.2.1  $\text{Ga}_2\text{O}_3$

# **Chapter 6**

## **Conclusion**

**6.1 Future direction**

**6.2 Concluding remarks**

# List of Figures

2.1	Process diagram for device fabrication . . . . .	8
2.2	CVD graphene grown on Cu transferred onto SiO <sub>2</sub> and Au pads. . . . .	8
2.3	Spin curve of AZ-1512HS . . . . .	10
2.4	Material remanants from lithography . . . . .	11
2.5	Bilayer lithography process . . . . .	11
2.6	Photolithography mask writing . . . . .	12
2.7	Developing an exposure array on SiO <sub>2</sub> . . . . .	12
2.8	Cleaning of graphene using UV Ozone . . . . .	13
2.9	E-beam Evaporation . . . . .	13
2.10	Deposition contacts . . . . .	14
2.11	PG Remover liftoff. . . . .	14
2.12	Ultrasonication used to remove material remnants from lithography. . . . .	14
2.13	Ultrasonication that has broken graphene sample. . . . .	15
2.14	Ag/H annealing . . . . .	15
2.15	PCB wafter mount . . . . .	15
2.16	Liquid metal oxide exfoliation . . . . .	16
2.17	Schematics of resistance measurements . . . . .	17
2.18	Instrumentation connections to a gated graphene FET . . . . .	18
2.19	LakeShore Probestation . . . . .	19
2.20	Probestation refrigerator . . . . .	19
2.21	Probestation micro-manipulated stages . . . . .	20
3.1	Ratio of G to 2D peaks in graphene and bilayer . . . . .	22
3.2	Raman 2D fitting of graphene and bilayer . . . . .	23
3.3	Raman processes in graphene . . . . .	23
3.4	RGB images of graphene on 285nm SiO <sub>2</sub> . . . . .	24
3.5	Contrast imaging sample 1 . . . . .	25
3.6	Contrast imaging sample 2 . . . . .	25

# List of Tables

# Chapter 7

## References

- [1] K. S. Novoselov, A. K. Geim, S. V. Morozov, D. Jiang, Y. Zhang, S. V. Dubonos, I. V. Grigorieva, and A. A. Firsov. Electric Field Effect in Atomically Thin Carbon Films. *Science*, 306(5696):666–669, October 2004.
- [2] Yi Zhang, Luyao Zhang, and Chongwu Zhou. Review of Chemical Vapor Deposition of Graphene and Related Applications. *Accounts of Chemical Research*, 46(10):2329–2339, October 2013.
- [3] Xuesong Li, Weiwei Cai, Jinho An, Seyoung Kim, Junghyo Nah, Dongxing Yang, Richard Piner, Aruna Velamakanni, Inhwa Jung, Emanuel Tutuc, Sanjay K. Banerjee, Luigi Colombo, and Rodney S. Ruoff. Large-Area Synthesis of High-Quality and Uniform Graphene Films on Copper Foils. *Science*, 324(5932):1312–1314, June 2009.
- [4] Changxi Zheng, Qianhui Zhang, Bent Weber, Hesameddin Ilatikhameneh, Fan Chen, Harshad Sahasrabudhe, Rajib Rahman, Shiqiang Li, Zhen Chen, Jack Hellerstedt, Yupeng Zhang, Wen Hui Duan, Qiaoliang Bao, and Michael S. Fuhrer. Direct Observation of 2d Electrostatics and Ohmic Contacts in Template-Grown Graphene/WS<sub>2</sub> Heterostructures. *ACS Nano*, 11(3):2785–2793, March 2017.
- [5] K. S. Novoselov, D. Jiang, F. Schedin, T. J. Booth, V. V. Khotkevich, S. V. Morozov, and A. K. Geim. Two-dimensional atomic crystals. *Proceedings of the National Academy of Sciences*, 102(30):10451–10453, July 2005.
- [6] Yuan Huang, Eli Sutter, Norman N. Shi, Jiabao Zheng, Tianzhong Yang, Dirk Englund, Hong-Jun Gao, and Peter Sutter. Reliable Exfoliation of Large-Area High-Quality Flakes of Graphene and Other Two-Dimensional Materials. *ACS Nano*, 9(11):10612–10620, November 2015.
- [7] Az1500 series technical datasheet.
- [8] EMD performance materials. Az 1500 series technical datasheet.
- [9] Jeongwon Park, Richard D. Yang, Corneliu N. Colesniuc, Amos Sharoni, Sungho Jin, Ivan K. Schuller, William C. Trogler, and Andrew C. Kummel. Bilayer processing for an enhanced organic-electrode contact in ultrathin bottom contact organic transistors. *Applied Physics Letters*, 92(19):193311, May 2008.
- [10] Microchem.com (2018). Pmgi and lor resists: Faqs :: Microchem., 2018.
- [11] Wei Li, Yiran Liang, Dangmin Yu, Lianmao Peng, Kurt P. Pernstich, Tian Shen, A. R. Hight Walker, Guangjun Cheng, Christina A. Hacker, Curt A. Richter, Qiliang Li, David J. Gundlach, and Xuelei Liang. Ultraviolet/ozone treatment to reduce metal-graphene contact resistance. *Applied Physics Letters*, 102(18):183110, May 2013.

- [12] A. Nath, A. D. Koehler, G. G. Jernigan, V. D. Wheeler, J. K. Hite, S. C. Hernndez, Z. R. Robinson, N. Y. Garces, R. L. Myers-Ward, C. R. Eddy, D. K. Gaskill, and M. V. Rao. Achieving clean epitaxial graphene surfaces suitable for device applications by improved lithographic process. *Applied Physics Letters*, 104(22):224102, June 2014.
- [13] Anindya Nath, Marc Currie, Anthony K. Boyd, Virginia D. Wheeler, Andrew D. Koehler, Marko J. Tadjer, Zachary R. Robinson, Karthik Sridhara, Sandra C. Hernandez, James A. Wollmershauser, Jeremy T. Robinson, Rachael L. Myers-Ward, Mulpuri V. Rao, and D. Kurt Gaskill. In search of quantum-limited contact resistance: understanding the intrinsic and extrinsic effects on the graphenemetal interface. *2D Materials*, 3(2):025013, 2016.
- [14] Understanding Thin Film Process TechnologiesREO Inc.
- [15] Yung-Chang Lin, Chun-Chieh Lu, Chao-Huei Yeh, Chuanhong Jin, Kazu Suenaga, and Po-Wen Chiu. Graphene Annealing: How Clean Can It Be? *Nano Letters*, 12(1):414–419, January 2012.
- [16] Daniel R. Cooper, Benjamin DAnjou, Nageswara Ghattamaneni, Benjamin Harack, Michael Hilke, Alexandre Horth, Norberto Majlis, Mathieu Massicotte, Leron Vandsburger, Eric White-way, and Victor Yu. Experimental Review of Graphene, 2012.
- [17] Caterina Soldano, Ather Mahmood, and Erik Dujardin. Production, properties and potential of graphene. *Carbon*, 48(8):2127–2150, July 2010.
- [18] Jian-Hao Chen, Chaun Jang, Shudong Xiao, Masa Ishigami, and Michael S. Fuhrer. Intrinsic and extrinsic performance limits of graphene devices on SiO<sub>2</sub>. *Nature Nanotechnology*, 3(4):206–209, April 2008.
- [19] Ali Zavabeti, Jian Zhen Ou, Benjamin J. Carey, Nitu Syed, Rebecca Orrell-Trigg, Edwin L. H. Mayes, Chenglong Xu, Omid Kavehei, Anthony P. OMullane, Richard B. Kaner, Kourosh Kalantar-zadeh, and Torben Daeneke. A liquid metal reaction environment for the room-temperature synthesis of atomically thin metal oxides. *Science*, 358(6361):332–335, October 2017.
- [20] Keithley Instruments. *Model 2400 Series SourceMeter User’s Manual*, 2400s-900-01 rev. g edition, May 2002.
- [21] Stanford Research Systems. *Model SR830 DSP Lock-In Amplifier*, 2.5 edition, October 2011.
- [22] R. P. Vidano, D. B. Fischbach, L. J. Willis, and T. M. Loehr. Observation of Raman band shifting with excitation wavelength for carbons and graphites. *Solid State Communications*, 39(2):341–344, July 1981.
- [23] R. J. Nemanich and S. A. Solin. First- and second-order Raman scattering from finite-size crystals of graphite. *Physical Review B*, 20(2):392–401, July 1979.
- [24] F. Tuinstra and J.L. Koenig. Characterization of Graphite Fiber Surfaces with Raman Spectroscopy. *Journal of Composite Materials*, 4(4):492–499, October 1970.
- [25] F. Tuinstra and J. L. Koenig. Raman Spectrum of Graphite. *The Journal of Chemical Physics*, 53(3):1126–1130, August 1970.
- [26] A. C. Ferrari, J. C. Meyer, V. Scardaci, C. Casiraghi, M. Lazzeri, F. Mauri, S. Pisacane, D. Jiang, K. S. Novoselov, S. Roth, and A. K. Geim. Raman Spectrum of Graphene and Graphene Layers. *Physical Review Letters*, 97(18):187401, October 2006.
- [27] Andrea C. Ferrari and Denis M. Basko. Raman spectroscopy as a versatile tool for studying the properties of graphene. *Nature Nanotechnology*, 8(4):235–246, April 2013.

- [28] P. Blake, K. S. Novoselov, A. H. Castro Neto, D. Jiang, R. Yang, T. J. Booth, A. K. Geim, and E. W. Hill. Making graphene visible. *Applied Physics Letters*, 91(6):063124, August 2007. arXiv: 0705.0259.
- [29] Hai Li, Jumiati Wu, Xiao Huang, Gang Lu, Jian Yang, Xin Lu, Qihua Xiong, and Hua Zhang. Rapid and Reliable Thickness Identification of Two-Dimensional Nanosheets Using Optical Microscopy. *ACS Nano*, 7(11):10344–10353, November 2013.
- [30] Ying Ying Wang, Ren Xi Gao, Zhen Hua Ni, Hui He, Shu Peng Guo, Huan Ping Yang, Chun Xiao Cong, and Ting Yu. Thickness identification of two-dimensional materials by optical imaging. *Nanotechnology*, 23(49):495713, 2012.
- [31] R. R. Nair, P. Blake, A. N. Grigorenko, K. S. Novoselov, T. J. Booth, T. Stauber, N. M. R. Peres, and A. K. Geim. Fine Structure Constant Defines Visual Transparency of Graphene. *Science*, 320(5881):1308–1308, June 2008.
- [32] A. B. Kuzmenko, E. van Heumen, F. Carbone, and D. van der Marel. Universal Optical Conductance of Graphite. *Physical Review Letters*, 100(11):117401, March 2008.
- [33] Z. H. Ni, H. M. Wang, J. Kasim, H. M. Fan, T. Yu, Y. H. Wu, Y. P. Feng, and Z. X. Shen. Graphene Thickness Determination Using Reflection and Contrast Spectroscopy. *Nano Letters*, 7(9):2758–2763, September 2007.

# Appendices

## **Appendix A**

### **Raman spectroscopy samples**

## Appendix B

### Labview programs